Experiments on Supersonic Jet Noise

J. Laufer,* R. Schlinker,† and R. E. Kaplan‡
University of Southern California, Los Angeles, Calif.

The noise generated by a 1-in. supersonic jet was investigated at nominal jet Mach numbers of 1.5, 2.0, and 2.5. In particular, a quantity $\bar{W}$, referred to as the apparent source strength per unit length, was determined along the jet axis using a directional microphone system. The integrated value of $\bar{W}$ along the jet axis was found to agree with the sound intensity obtained by a conventional microphone. This result is consistent with the a priori assumption that the jet may be described in terms of independent, spatially compact acoustic sources. The main finding of the investigation is the discovery of two distinct intense noise-producing regions in a jet having supersonic source velocities: the upstream region associated with Mach wave radiation, and a zone, located downstream of the potential cone, exhibiting radiation similar in character to that of a subsonic jet. An estimate of the radiated intensity associated with the Mach waves also is made.

Introduction

A GREAT amount of effort has been spent in studying the supersonic jet noise problem in the past decade. The primary concentration of most of these studies was more on developing effective noise suppressors than on the understanding of the mechanism itself. It is becoming apparent, however, that, because of the complicated nature of the radiation phenomenon, more fundamental experiments are needed in order to be able to understand the physics of the radiation, and then to attack the noise-abatement problem. This point of view motivated the work described in this paper; fully expanded jets, with room stagnation temperatures, have been used in order to investigate experimentally the nature and axial location of the most intense noise-producing regions.

There are a number of theoretical analyses in the literature dealing with the noise generated by supersonic jets, some of which were most helpful in the formulation and interpretation of the present experiments. The first treatment addressing itself directly to the high Mach number noise radiation problem is that of Phillips.[1] He predicted that turbulent shear layers with supersonic convection velocities, relative to that of the acoustic medium, radiate in the form of Mach waves. Subsequently, Ffowcs Williams[2] and Ribner[3] gave a similar interpretation within the framework of their acoustic analogy. More recently, Liu[4] and Tam[5] proposed noise-generation mechanisms based on two different types of shear layer instability. Most of these analytical considerations suggest that special attention will have to be given to regions where the source velocities are expected to be supersonic with respect to the medium.

Indeed, a number of shadowgraphs and Schlieren observations have been made indicating the Mach wave nature of the radiation. More recently, Salant[6] and Ozkul[7] applied a holographic interferometer technique with which the instantaneous spatial distribution of the density field can be obtained, in both the near and far field. Two significant comments can be made on the basis of these studies: first, from the three-dimensional view of the holograms, the wave fronts appear conical; second, the waves seem to originate from large-scale disturbances, clearly visible around the supersonic potential core, but are not observed downstream of the core tip.

A number of quantitative experiments have attempted to determine the location and nature of the dominant noise sources with varying success. One of the more innovative approaches was suggested by Potter[8] and also applied by McGregor and Simcox.[9] Experimentally, this involved retracting a jet into a sound-isolating cell in incremental steps while measuring the sound radiated by that portion of the jet still outside the cell. With this relatively crude technique, the average acoustic power output per unit length of the jet was obtained, and the maximum power output was located at approximately 20 jet diameters for $M_j = 2.5$, a result not different from that of the present work.

A more sophisticated method, the acoustic imaging technique applied for jet noise studies, was suggested first by Grosche in a report presenting some qualitative results uncorrected for diffraction effects.[10] The first quantitative data applied to subsonic jets were given by Laufer et al.[11] The work described here extends their results to supersonic jet Mach numbers in the range of 1.5 to 2.5. The two most interesting results of the investigation show first that there are, in fact, two distinct intense noise-producing regions in a jet having supersonic source velocities, and, second, the upstream region radiates in the form of Mach waves, producing very characteristic pressure signatures in the far field. This latter observation was made independently and concurrently by Ffowcs Williams.[12]

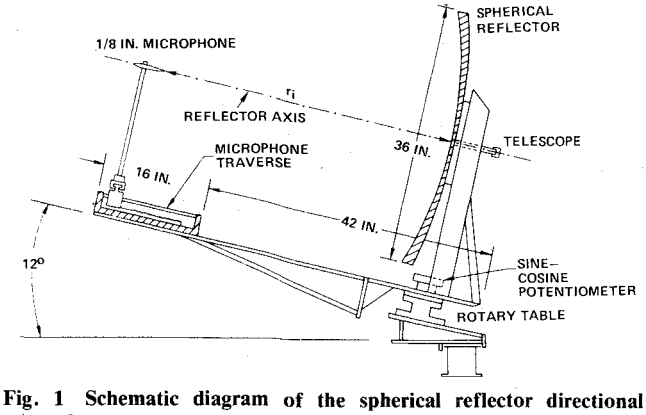

Fig. 1 Schematic diagram of the spherical reflector directional microphone system.

Presented as Paper 75-478 at the AIAA 2nd Aero-Acoustics Conference, Hampton, Va., March 24-26, 1975; submitted March 27, 1975; revision received September 2, 1975. The authors gratefully acknowledge the generous support of the Department of Transportation under Grant DOT-OS-00002. Assistance by United Aircraft in the preparation of the final figures is greatly appreciated.

Index category: Aircraft Noise, Aerodynamics (Including Sonic Boom).

*Professor of Aerospce Engineering. Fellow AIAA.

†Research Assistant, Aerospace Engineering; presently Research Engineer, United Technologies Research Center, East Hartford, Conn. Member, AIAA.

‡Professor of Aerospace Engineering.

Experimental Apparatus and Procedure

The anechoic chamber at the USC Jet Noise Laboratory has a 244- × 188- × 143-in. free-field volume. The chamber and the blowdown jet facility are described in detail in Ref. 13.

The directional microphone system shown in Fig. 1 uses the imaging property of a spherical reflector. The reflector used in this work has a 53-in. radius of curvature and a 36-in. aperture. The dimensions are based on the results of a parametric study of spherical reflectors.[14] A ⅛-in. B and K condenser microphone measures the focused energy at the image point. The entire directional microphone system can be moved parallel to the jet axis on the track shown in Fig. 2. The motorized rotary table allows the system to turn and automatically scan along the jet axis from a fixed position in the far field. The scanning is controlled by a special electronic command described in detail in Ref. 13.

In order to determine the optimum pressure ratio for a given nozzle, a series of shadowgraphs was taken near the design stagnation pressure. The optimum Mach number and pressure ratio were based on the criterion that the deflection angles of the weak intersecting compression waves, emanating from the nozzle lip, be minimal. In all cases, the bounding shear layers of the flow were straight, and no shock cells were visible. Figure 3 shows the flowfield in the first 3 diam downstream of the exit for the $M_j = 2.5$ nozzle.

The exact values of the shock-free exit Mach numbers M_E of the experiments were found to be 1.47, 1.97, and 2.47. The corresponding stagnation pressures were 51.7, 109.7, and 239.7 psia, respectively. The average ambient pressure was 14.7 psia.

Acoustic data were recorded beginning 1-3 min after the valve was opened, the lag time being necessary for the stagnation pressure to be brought to within ± 1% variation. With a run time of 7 min required for the directional microphone to scan 64 points on the jet axis, a maximum temperature drop of 10°-25°F (relative to the stagnation temperature at $t = 0$) could occur, depending on the Mach number. In terms of an absolute temperature change, this corresponds to a 1.8%-4.7% decrease. The changes in the settling chamber stagnation pressure and temperature changed the jet exit speed by approximately 1%-2.4%, corresponding to a 0.3-0.7 dB change in the measured intensity.

Figure 2 shows the experimental setup including two omnidirectional microphones. The inserted table indicates the experimental conditions. Once the operating pressure range was reached, the tape recorder and automatic scanner were started. The directional microphone output measured at each axial station was amplified, filtered, and recorded while a second channel recorded the unfiltered signal. (A filter with a frequency response proportional to f^{-2} was used in order to balance out the f^2 type of gain, characteristic of the directional microphone discussed in the following section.) The 90° and oblique angle omnidirectional microphone signals also were put on tape. All acoustic data were recorded on direct channels, whereas the reflector controller output and the settling changer pressure were recorded on FM channels. A marker pulse, provided by the controller each time the reflector stopped to a new position, also was recorded on FM. This was used later in the data-processing scheme.

The typical run lasted 7 min.. with approximately 6.3 sec between reflector steps. During the run, the average anechoic chamber temperature was 72°F, with a range of approximately ±5°F. Also, the average humidity was 45%, with a variation of ±5%.

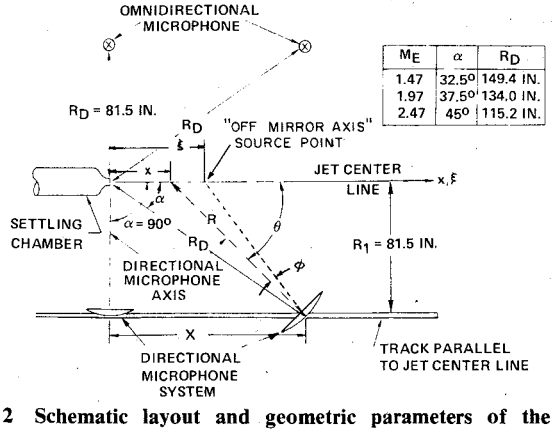

Fig. 2 Schematic layout and geometric parameters of the experiment.

Theory and Application of the Directional Microphone

The reflector-type directional microphone can be characterized as a receiver that is most sensitive to acoustic source located along its axis. The axis of the system defines a unique direction. Points off the axis are defined by the angle ϕ. Although the system may be designed optimally, it is diffraction-limited, especially near the low-frequency spectral peak of typical jet noise. As noted in Ref. 11, the parameter governing diffraction is

$$\eta = (\pi D/\lambda)\sin\phi \tag{1}$$

where D is the reflector diameter, and λ is the acoustic wavelength. In terms of η, the response I to an ideal omnidirectional point source of strength S_0 at a distance R_D is then

$$I(\eta, \lambda/D, R_d) = (S_0/4\pi R^2)G(\lambda/D)H(\eta) \tag{2}$$

where $G(\lambda/D)$ describes the frequency-dependent gain, and $H(\eta)$, usually referred to as the window function, describes the directional characteristics of the reflector system.

For an ideal system without diffraction, G is proportional to the solid angle subtended by the reflector so that

$$G = (D/d)^2 \tag{3}$$

where d is the image point microphone diameter. Also, $H(\eta)$, for such an ideal system, is a Dirac delta function centered at $\eta = 0$.

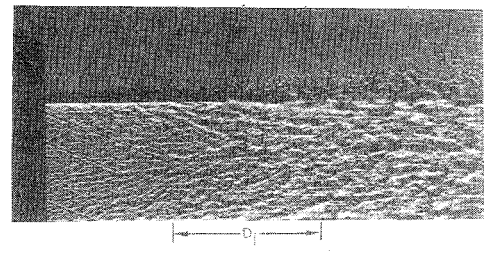

Fig. 3 Shadowgraph of the flowfield and acoustic radiation for the $M_E = 2.47$ converging-diverging nozzle.

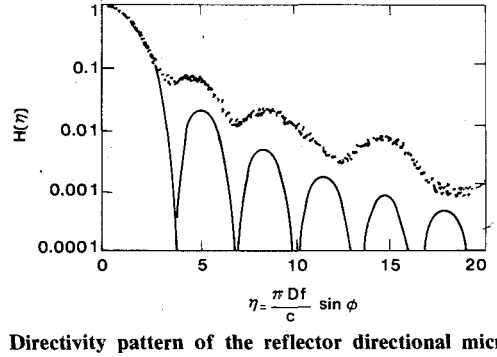

Fig. 4 Directivity pattern of the reflector directional microphone system:——Fraunhofer diffraction pattern; ..... measured diffraction pattern.

If one considers the directivity of the reflector system to be defined by the Fraunhofer diffraction theory for a circular aperture, then, given a zero bandwidth detector,

$$H(\eta) = [2J(\eta)/\eta]^2 \tag{4}$$

Equation (4) holds strictly for sources located at infinity on the reflector axis. Figure 4 shows the response predicated by (4) for $D=3$ ft, $d=\frac{1}{8}$ in. The figure also indicates the experimentally determined window function, using a point source of random sound[11] at a finite distance of $R=8.5$ in. The normalized pressure spectral density response has been plotted vs the diffraction parameter η. The data were obtained over a frequency range of 1-100 kHz, using 500-Hz bandwidths. The response agrees generally with that predicted by (4), over the range $0 \leq \eta \leq 3$, which turns out to be within the limits of the present experiments.

As previously mentioned, the ideal system would have a gain $G=(D/d)^2$ in the geometrical limit. This expression, however, is altered by diffraction. It can be shown[11] that, by using a low-frequency (small η) approximation, the gain function can be calculated explicitly and has the following form:

$$G = \tfrac{1}{4}\{(\pi D^2 f/2Rc)[(2R-R_m)/R_m]\}^2 \tag{5}$$

where R_m is the mirror radius of curvature. (The equation in Ref. 11 lacks a factor of ½.) The f^2 gain dependence, mentioned earlier, is apparent from Eq. (5). Thus, the total measured signal will be weighted heavily by the high-frequency region of the noise spectrum. This causes the low-frequency portion to be lost in the recording system noise, unless the high-frequency dominance is balanced out. This was done by using a filter amplifier with a gain proportional to f^{-2}.

The form of G was determined experimentally by Kao[15] and is shown in Fig. 5. The experimental gain in Fig. 5 displays the predicted f^2 dependence at low frequencies. In fact, when extended down to 1 kHz, it agrees absolutely with the theoretical gain $G(f=1\times10^3 \text{ Hz})=4.0$ at $\alpha=90°$, $R_D=81.5$ in. However, beyond $f=6$ kHz, $G_{\exp} \sim (f)f^{1.5}$, as shown by the dotted line fitted through the experimental data points.

In the data analysis the following form of the gain function has been adopted:

$$G'(f) = \begin{cases} G(f) & \text{for } f \leq f_1 = 6\text{kHZ} \\ G(f)[f/f_1]^{1.5} & \text{for } f \geq f_1 = 6\text{kHz} \end{cases} \tag{6}$$

Here $G(f)$ is the previously discussed theoretical gain, based on the dice to the central aiming point. It should be mentioned that the calibration curve was extrapolated to about 100 kHz, the frequency limit of the present experiment, in the process of the data analysis. The internal consistency of the final results justifies this procedure.

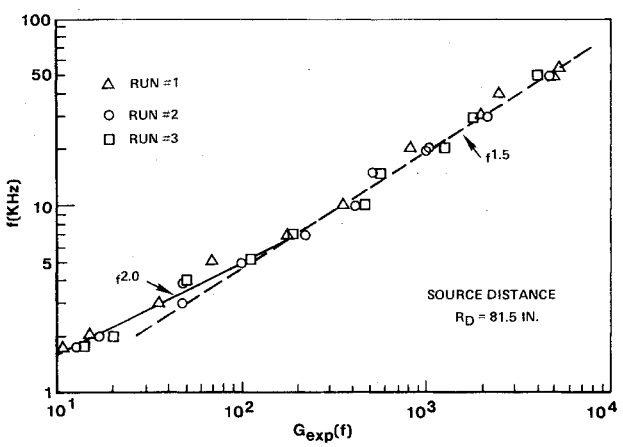

Fig. 5 Experimental gain of the reflector directional microphone.

We may define a quantity $\tilde{W}$ in terms of the following integral equation, involving the radiated intensity at a given point X, R_D:

$$I(X,R_D) \equiv \overline{p^2}/\rho c = \int_0^{+\infty} \frac{\tilde{W}}{4\pi R^2}\,dx \tag{7}$$

The quantity $\tilde{W}$ may be interpreted as an apparent or equivalent source strength per unit length, sensed by a narrow-angle microphone placed in the far field. $\overline{p032}$ is the mean square of the pressure fluctuations in the far field. Paramount to the formulation of Eq. (7) is the condition that the sces located on the jex axis are uncorrelated with neighboring ones, within the limits of resolution of the measurements. Thus, no phase cancellation occurs at the image point because of adjacent sources. Also implicit in the formulation is that the window function is wider than the local jet diameter at the frequency of interest. These assumptions will be justified, a posteriori, by the internal consistency of the measurements.

If the spectral density of the apparent source is represented as $W(x,f,\theta)$, then the filtered spectral density of the acoustic pressure, $\psi(x,f)$, measured in the far field with the directional microphone located at X, R_D, and aimed at point x, is related to $W(x,f,\theta)$ by the integral equation:

$$\psi(x,f) = \rho c G'(f) \int_{-\infty}^{+\infty} H'(\eta)\,\frac{W(\xi,f,\theta)}{4\pi R^2}\,d\xi + \rho c \int_{-\infty}^{+\infty} A(\xi,f)\,\frac{W(\xi,f,\theta)}{4\pi R_2^2}\,d\xi \tag{8}$$

where

- ρ = ambient density of air
- c = ambient speed of sound
- G' = frequency-dependent gain of the reflector
- ξ = position coordinate along x of the "off-mirror axis" source
- H' = finite bandwidth reflector window function; $H'(0)=1$
- W = spectral density of the apparent source strength per unit length emitting in the direction θ
- A = microphone shielding function
- R = distance between the mirror and the source point
- R_2 = distance between the microphone and the source point

$$H'(\eta) = \frac{\int_{-\infty}^{+\infty} \left(\frac{2J_1(\eta)}{\eta}\right)^2 a(\gamma-f)\,d\gamma}{\int_{-\infty}^{+\infty} a(\gamma-f)\,d\gamma} \tag{9}$$

Here $a(\gamma-f)$ corresponds to the power transfer function of the filter used. The second integral in Eq. (8) accounts for the direct radiation from the jet arriving at the focal point microphone. When the system is aimed far upstream of the nozzle exit or downstream beyond the significant noise-producing region, the contribution of the direct radiation is no longer negligible and is expressed in the form of the shielding term $A(x,f)$. For an ideal omnidirectional microphone without shielding, $A(x,f)=1$. Although this may seem like a satisfactory engineering approximation, experience has shown that it gives a poor estimate of the response to the direct radiation. The approach adopted to solve this problem was an iterative consistency method discussed in detail in Ref. 13.

One of the major tasks of this study was the recovery of $W(x,f,\theta)$ in Eq. (8) from the measured spectrum ψ. Three

methods have been investigated for solving Eq. (8) to obtain an optimal spatial resolution: 1) an integral transform technique as used in Ref. 16, 2) a matrix inversion technique as used in Ref. 11, and 3) an interative technique as used in Ref. 17. A detailed study of each technique was reported in Ref. 17. The results indicated that the iterative technique is best able to recover the amplitude and structure of the axial power distribution. Thus, it was chosen as the standard method in this work. The digital data reduction, frequency response correction, presmoothing, and other corrections are described in some detail in Ref. 13.

Results and Discussion

Spatially Coherent, Independent Sources

A basic requirement for $\tilde{W}$ to be a physically meaningful quantity is that flow regions of a certain limited size exhibit spatial coherence over a finite time period and behave independently as acoustic sources. Although this notion was suggested and used by Lighthill in estimating his volume integral,[18] no direct experimental evidence exists so far to substantiate its validity. In fact, the so-called linear antenna theory of Crow[19] does not accept this assumption.

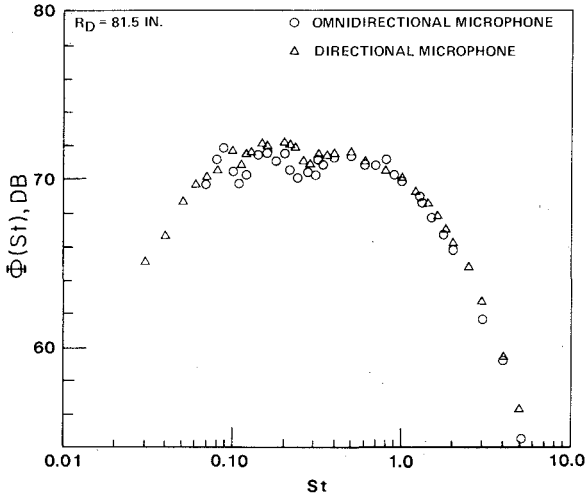

Fig. 6 Comparison of omnidirectional and directional microphone measurements in terms of the narrow-band spectral density of the pressure fluctuations $\Phi(St)$ expressed in decibels (re 0.0002 dyne/cm^2); $M_E = 1.97$, $\alpha = 90°$.

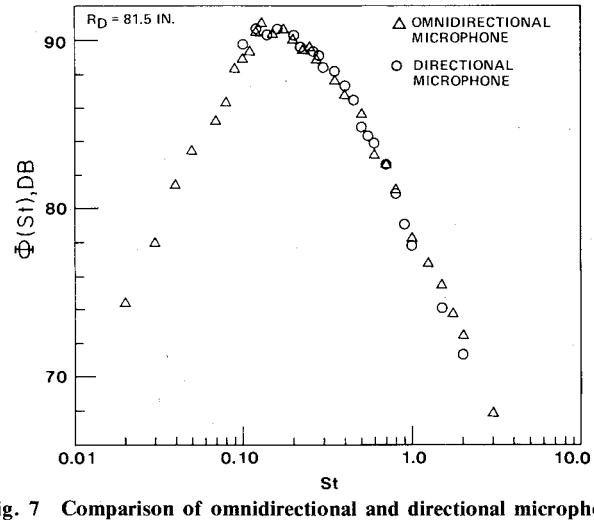

Fig. 7 Comparison of omnidirectional and directional microphone measurements in terms of the narrow-band spectral density of the pressure fluctuations $\Phi(St)$ expressed in decibels (re 0.0002 dyne/cm^2); $M_E = 1.97$, $\alpha = 37.5°$.

Since this notion is of great general importance, and since the directional microphone technique is critically dependent on its validity, it is necessary to show that the results obtained with this method are, in fact, consistent with the concept that the turbulent jet, viewed as a source of noise, is the summation of a number of independent acoustic sources distributed along the jet axis. Accordingly, the relationship expressed by Eq. (7) has to be confirmed by independent measurements of the mean square pressure fluctuations, using an omnidirectional microphone, and of the axial apparent source strength per unit length distribution measured using a directional microphone. In actuality, the spectral densities of these quantities were obtained. Thus, at a point X, R_D,

$$\Phi(f,X,R_D) = \rho c \int_0^\infty \frac{W(x,f,\theta)}{4\pi R^2} \tag{10}$$

where

$$\overline{p^2} = \int_0^\infty \Phi(f)\,df, \quad \tilde{W} = \int_0^\infty W(f)\,df \tag{11}$$

A typical comparison of Φ (obtained with an omnidirectional microphone) with the right-hand side of Eq. (10), evaluated from Eq. (8) and measurements of ψ, using the directional microphone, is given in Figs. 6 and 7. The nondimensional frequency St is defined in terms of D_j and U_E. The agreement is considered satisfactory. Furthermore, the overall intensities [Eq. (7)] obtained by the two methods also agree within 1 dB in all cases. These results provide confidence in the accuracy of the data-processing scheme, as well as in the validity of the basic assumptions involved in the technique. On the basis of these results, it may be concluded that: *the notion of independent, spatially coherent sources distributed along the jet axis is a realistic and useful description of the acoustic behavior of a supersonic jet flow.*

Features of the Far-Field Intensity

Figure 8 shows the distributions of the normalized spectral density $\Phi/\overline{p^2}$ obtained for $\alpha = 90°$ at three different Mach numbers, plotted in a nondimensional form. U_E/D_j is used, as is customary, for the characteristic frequency. It is seen that, although the shapes of the distributions are approximately the same, the spectra do not scale with this frequency, contrary to subsonic jets. This can be explained in terms of the compressibility effects on the mixing rates in a turbulent sheer layer. It is well known that subsonic jets are geometrically similar, because the principle of Reynolds

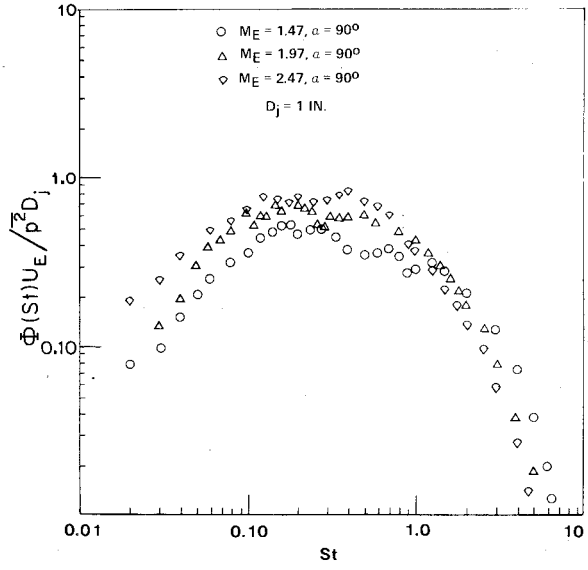

Fig. 8 Comparison of the normalized spectral density distributions of the pressure fluctuations at $\alpha = 90°$ for various M_E.

similarity holds over the major portion of the flow, and because compressibility effects are negligible on the turbulent processes in the field. As a consequence, the characteristic frequency is independent of both Reynolds and Mach numbers.

At supersonic speeds, the turbulent transport processes are less efficient, and the development time of the jet or its spreading rate will be affected by the flow Mach number. It is suggested, therefore, that the nondimensional scaling be defined as follows:

$$St' \equiv fL_1/U_E/ = St(L_1/D_j) \tag{12}$$

where L_1 is the location of the potential cone apex. The values of L_1 were obtained from Ref. 21. With this scaling, the three distributions of Fig. 8 indeed can be collapsed in a quite satisfactory manner as shown in Fig. 9. The figure also shows good agreement with the subsonic results of Lush and Burrin.[20] It should be mentioned, however, that the two slight peaks appearing in the supersonic data are believed to be real; their significance is presently under investigation.

Figure 10 compares the fair-field intensity spectrum measurements obtained at various oblique angles, corresponding approximately to the direction of maximum radiation intensity. The distributions are considerably different, and it is clear that the radiation fields in the three cases must be sufficiently dissimilar that no single characteristic time scale could describe them adequately. This conclusion will be discussed further, on the basis of results obtained with the directional microphone.

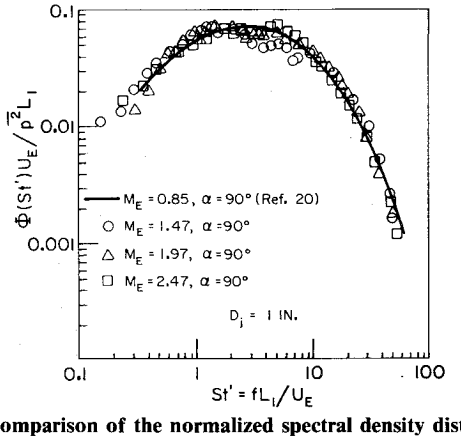

Fig. 9 Comparison of the normalized spectral density distributions of the pressure fluctuations at $\alpha = 90°$ for various M_E using the potential core length as a scaling parameter.

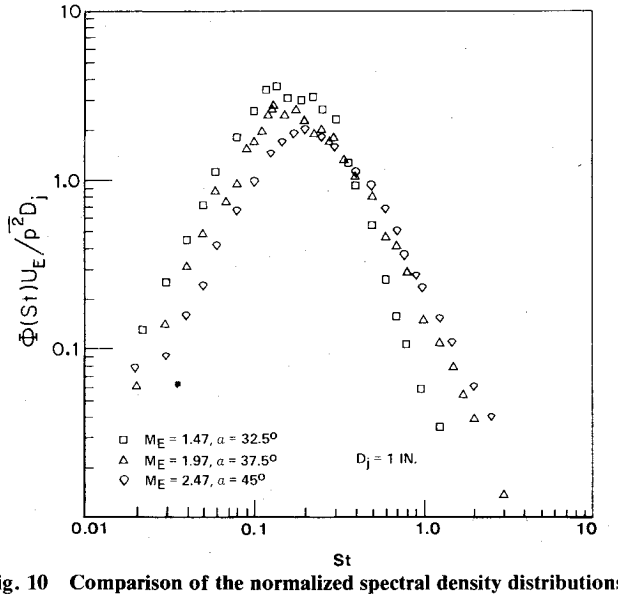

Fig. 10 Comparison of the normalized spectral density distributions of the pressure fluctuations at oblique angles for various M_E.

Apparent Axial Source Strength Distributions

Following the procedure discussed in the previous section, the apparent source strength per unit length distribution along the jet axis was obtained with the use of the directional microphone. Figures 11-13 show these distributions (normalized by the maximum value) for the three Mach number cases at $\alpha = 90°$. The axial positions L_1 and L_2 indicate,

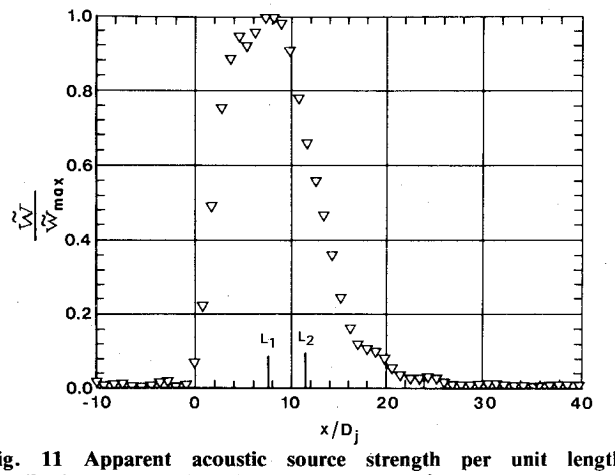

Fig. 11 Apparent acoustic source strength per unit length distribution along the jet axis; $M_E = 1.47$, $\alpha = 90°$.

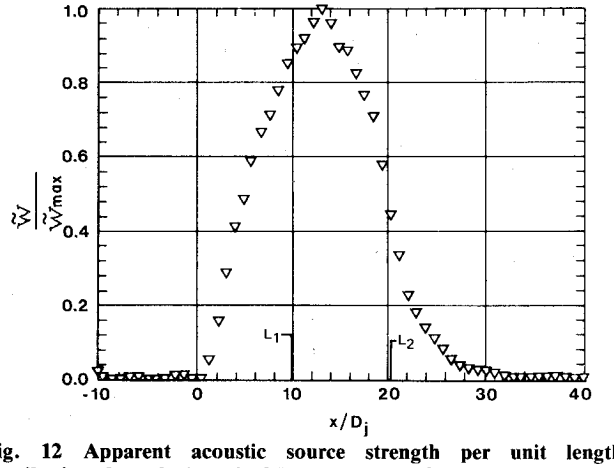

Fig. 12 Apparent acoustic source strength per unit length distribution along the jet axis; $M_E = 1.97$, $\alpha = 90°$.

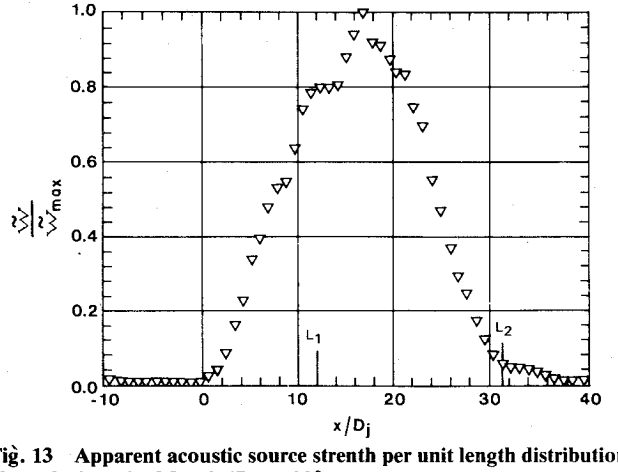

Fig. 13 Apparent acoustic source strenth per unit length distribution along the jet axis; $M_e = 2.47$, $\alpha = 90°$.

respectively, the locations of the potential cone apex and the centerline sonic point, based on the measurements of Nagamatsu et al.[21] The $\tilde{W}$ distributions look similar to those obtained for subsonic jets,[22] with two notable differences. First, the location of the maximum value shifts farther downstream with increasing Mach number; and second, the extent of the radiation region increases considerably, from 20 to about 25 diam, as the jet Mach number changes from 1.5 and 2.5. These differences are consistent with the notion that, for $\alpha \geq 90°$, the radiation is primarily caused by subsonically moving sources, and, as in subsonic jets, the most intense radiation emanates from the so-called transition zone, just downstream of the potential cone apex, a zone that shifts downstream with increasing Mach number.

The character of the radiation appears considerably different at observation angles corresponding approximately to the direction of maximum intensity of radiation. Figures 14-16 show the source strength distribution at $M_j = 1.5$, 2.0, and 2.5. Of particular interest is the one obtained at $M_j = 2.0$ (Fig. 15), where two distinct regions of intense radiation are observed. In order to investigate further this unexpected result, it is useful to discuss the spectral density distribution of the source strength along the jet axis. An advantageous way to

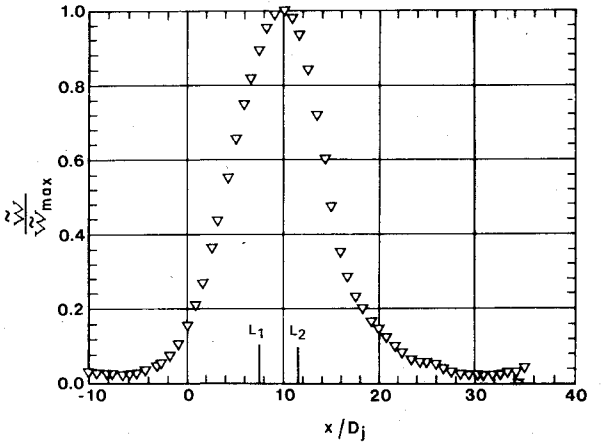

Fig. 14 Apparent acoustic source strength per unit length distribution along the jet axis; $M_E = 1.47$, $\alpha = 32.5°$.

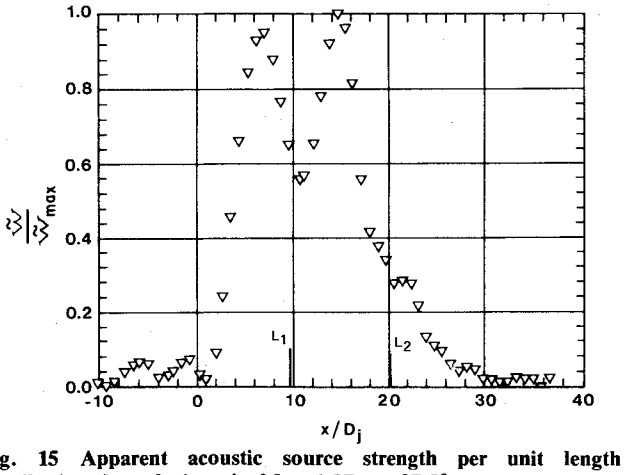

Fig. 15 Apparent acoustic source strength per unit length distribution along the jet axis; $M_E = 1.97$, $\alpha = 37.5°$.

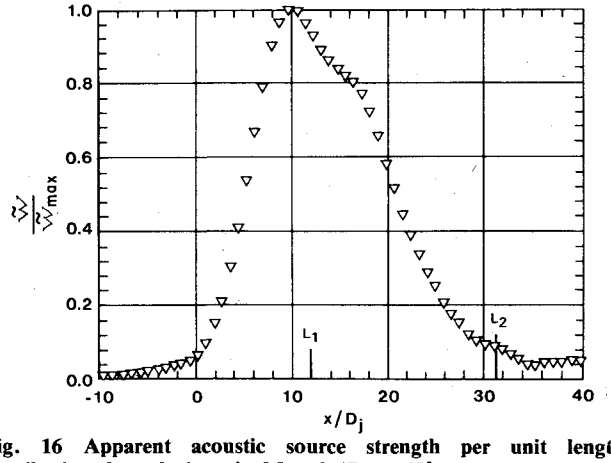

Fig. 16 Apparent acoustic source strength per unit length distribution along the jet axis; $M_E = 2.47$, $\alpha = 45°$.

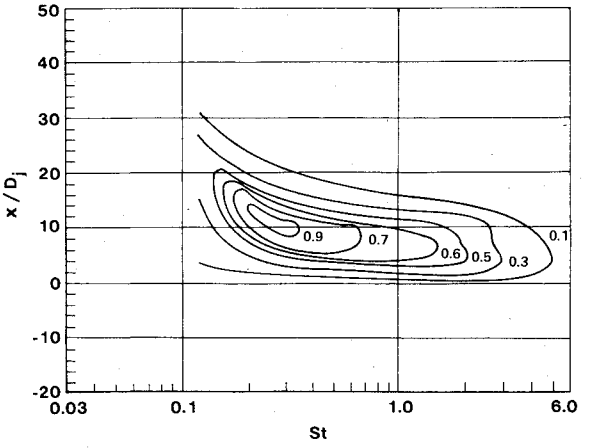

Fig. 17 Equal spectral density contours of the normalized apparent acoustic source strength per unit length; $M_E = 1.47$, $\alpha = 90°$.

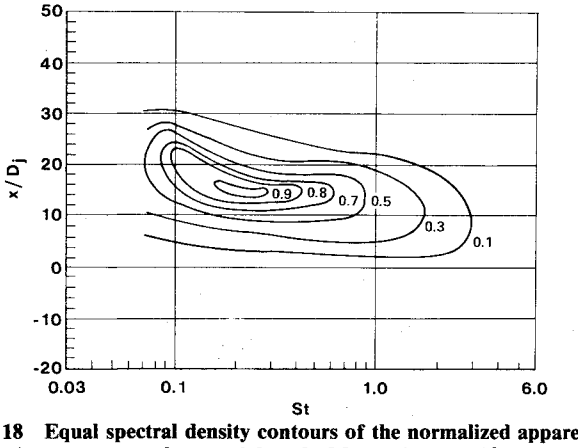

Fig. 18 Equal spectral density contours of the normalized apparent acoustic source strength per unit length; $M_E = 1.97$, $\alpha = 90°$.

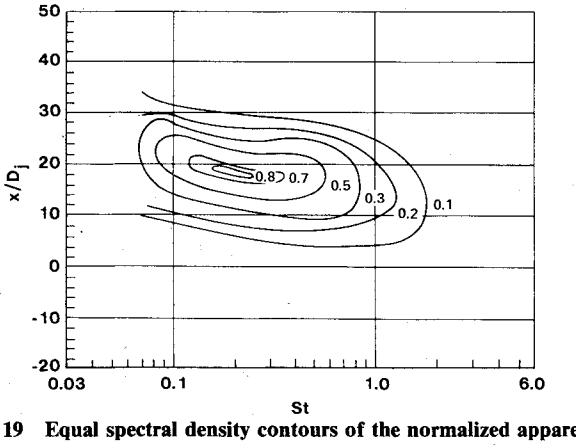

Fig. 19 Equal spectral density contours of the normalized apparent acoustic source strength per unit length; $M_E = 2.47$, $\alpha = 90°$.

exhibit these distributions is by showing lines of constant spectral density in the x/D_j Strouhal number plane. For $\alpha = 90°$, the shapes of the contour lines are again similar to those at subsonic Mach numbers (Figs. 17-19). In fact, if the scaling is changed, as suggested in the previous section, the contours would show even greater similarity.

However, the contour lines of constant spectral intensity show a completely different picture when the measurements are made at the oblique angles (Figs. 20-22). The spectral intensity has two distinct peaks at the two highest Mach numbers jets: a high-frequency peak emanating nearer the nozzle and a low-frequency one originating from sources farther downstream. The two peaks are especially distinct for the $M_j = 2$ jet and are exhibited well in a three-dimensional plot (Fig. 23). It is to be noted that, with increasing jet Mach number, the relative intensity of the high-frequency peak increases, and the two peaks tend to merge. Figure 23 also exhibits some wavy character of the spectrum, the significance of which is presently under study. These results clearly indicate that, at the higher Mach numbers, the radiation field exhibits new features, and they suggest that the problem should be examined in terms of the Mach wave generation mechanism of Phillips.

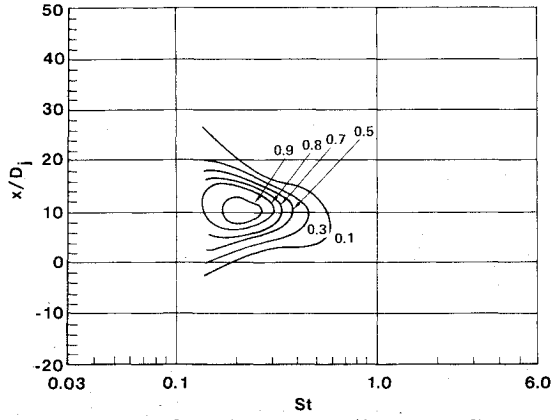

Fig. 20 Equal spectral density contours of the normalized apparent acoustic source strength per unit length; $M_E = 1.47$, $\alpha = 32.5°$.

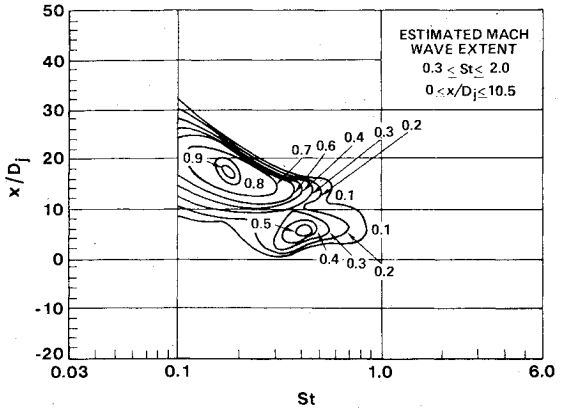

Fig. 21 Equal spectral density contours of the normalized apparent acoustic source strength per unit length; $M_E = 1.97$, $\alpha = 37.5°$.

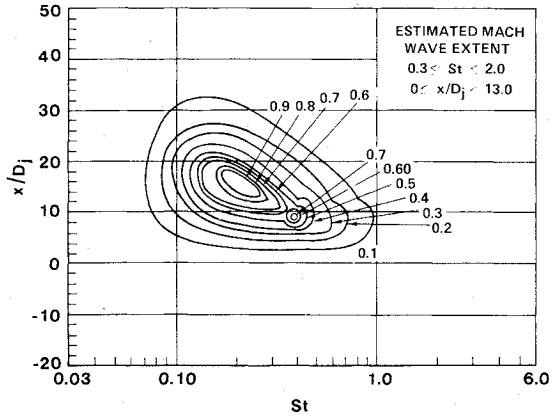

Fig. 22 Equal spectral density contours of the normalized apparent acoustic source strength per unit length; $M_E = 2.47$, $\alpha = 45°$.

Character of the Mach Wave Radiation

As indicated in the Introduction, optical observations have already been made of Mach waves originating from supersonic jets. However, no systematic quantitative studies of this phenomenon have been carried out so far. Perhaps the most dramatic indication of the presence of relatively strong pressure pulses having a characteristic shape have been obtained with the directional microphone. A time trace of such a signature is shown in Fig. 24a. (It is to be remembered that the microphone strongly emphasizes the high frequencies, gain $\sim f^2$, and that the pressure pulses are exaggerated.) For this

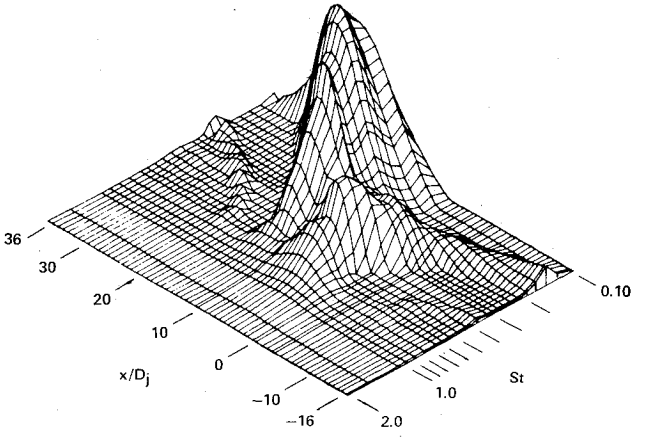

Fig. 23 Spectral density distribution of the apparent acoustic source strength per unit length along the jet axis and as a function of Strouhal number; $M_E = 1.97$, $\alpha = 37.5°$.

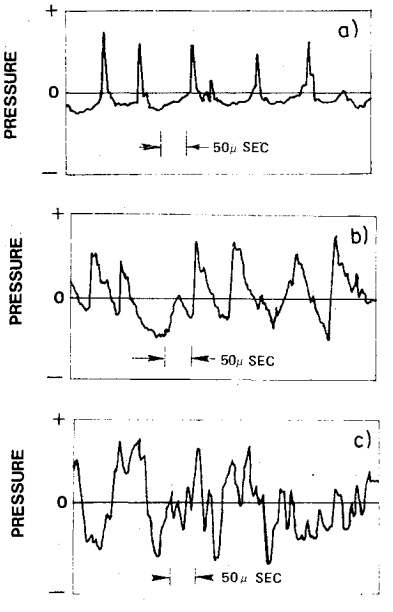

Fig. 24 Typical signals: a) directional microphone signal, $M_E = 2.47$, $\alpha = 45°$; b) omnidirectional microphone signal, $M_E = 2.47$, $\alpha = 45°$; c) omnidirectional microphone signal, $M_E = 2.47$, $\alpha = 90°$.

particular case $\alpha = 45°$. As the microphone axis is rotated away from this angle, in either direction, the spikes rapidly decrease.

Figures 24b and 24c show the pressure signatures obtained by an omnidirectional microphone at $\alpha = 45°$ and 90°. The difference in the two traces is quite striking. In the upper trace strong positive pressure gradients are exhibited repeatedly, followed by a milder pressure fall with the positive pressure peaks always higher than the minima, thus giving a skewed probability distribution. The lower trace, on the other hand, has nearly a gaussian distribution and is similar to that obtained in the far field of a subsonic jet. It is of interest to point out that similar observations have been made concurrently by Ffowcs Williams,[12] using a full-scale jet engine. Although his measurements of the skewness factor show somewhat higher values than those of the present work (possibly because of the elevated stagnation temperature), it is significant that a small diameter, clean, model jet reproduces the phenomenon observed with a full-sized, production-type hot jet engine.

It is reasonable to assume that the characteristic signatures that appear only within a limited range of θ (corresponding to the Mach wave directions observed by optical techniques) are associated with the Mach waves radiated by the jet. In order to study, in more detail, the shape of the pressure signals and to be able to estimate the amount of radiated energy carried by these waves, an education technique was developed. Taking advantage of the characteristic large positive gradients and high positive pressure peaks, a conditional sampling method was used to obtain an ensemble average of the characteristic wave shape. The method is described in detail in Ref. 13. It is of interest to note that a Fourier transform of this shape shows a spectral energy peak occurring at the same frequency as the second spectral peak seen in the contour plot (Fig. 21). This result further justifies attributing the second spectral peak to Mach wave radiation. By calculating the mean square value of the characteristic signal and by observing the fraction of time of its occurrence, the average intensity of the Mach waves could be estimated. It was found that, at $M_j = 2.0$, this intensity is approximately 30% of the measured total intensity. The same result was obtained by estimating the energy contained under the second spectral peak in Fig. 21.

A Qualitative Description of the Radiated Field

The general picture that emerges from the measurements carried out in the far field of a cold supersonic jet may be described in terms of two distinct types of radiation sources. One consists of spatially coherent structures, moving supersonically with respect to the medium and radiating highly directional Mach waves during their period of coherence. The waves arrive at random intervals at a given far-field point, generating a rather wide band spectrum. However, the rapid variation of the pressure across the wave produces relatively more energy in the high frequencies. This explains, to a large extent, the difference in the three spectral density distributions shown in Fig. 10. The significantly higher relative energy content at high frequencies for the two high Mach number jets is clearly observable. This picture also suggests that the radiation must be associated with at least two characteristic time scales: the low-frequency spectrum is expected to scale with the average period between waves, whereas the scale of the high-frequency spectrum should depend on the rapid pressure rise and, therefore, on the jet Mach number. The second type of radiation emanates from the subsonically moving sources located farther downstream and exhibits features much like subsonic jets. In particular, at $\alpha = 90°$ the noise intensity varies closely to the eighth power of the velocity (Fig. 25). Furthermore, the most intense radiation emanates from the so-called transition zone of the jet, just downstream of the potential cone. Finally, the normalized spectral densities exhibit a nearly self-similar distribution that agrees fairly well with that measured in a subsonic jet (Fig. 9).

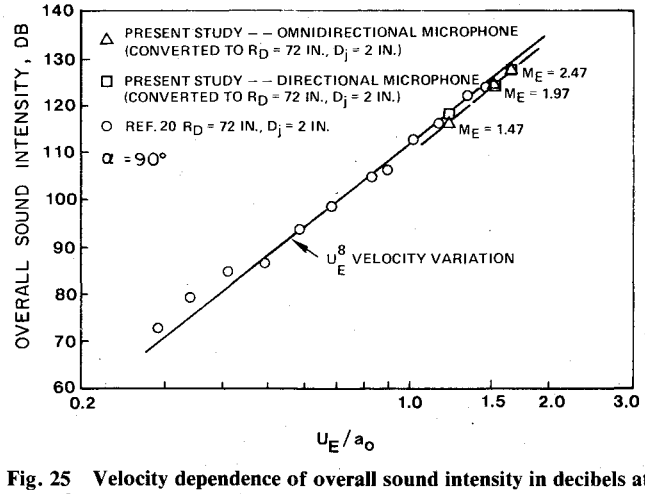

Fig. 25 Velocity dependence of overall sound intensity in decibels at $\alpha = 90°$.

Conclusions

The results presented in this paper show that the directional microphone system is an extremely useful tool in studying jet noise. With proper application, it gives much more detailed information than a conventional microphone. The principal conclusions obtained with the system may be summarized as follows:

1) Independent, spatially coherent sources distributed along the jet axis is a realistic and useful description of the acoustic behavior of a supersonic jet flow.

2) Measurements of the source strength per unit length distributions show conclusively that there are, in fact, two distinct intense noise-producing regions in a jet having supersonically convected sources.

3) Specially developed conditional sampling techniques prove that one of these regions, located upstream, radiates in the form of Mach waves characterized by strong high-frequency noise.

4) In the direction of the Mach wave radiation, 30-40% of the intensity is generated by the Mach wave radiation at $M_E = 2.0$.

5) The second strong noise-producing region located farther downstream has a radiation field similar to that found in subsonic jets. In particular, at $\alpha = 90°$, the intensity follows closely the eighth power law of the velocity, and its normalized spectral distribution, expressed in terms of a properly chosen dimensionless frequency, agrees with that of a subsonic jet.

References

[1] Phillips, O.M., "On the Generation of Sound by Supersonic Turbulent Shear Layers," *Journal of Fluid Mechanics,* Vol. 9, Pt. 1, 1960, pp. 1-28.

[2] Ffowcs Williams, J.E., "The Noise from Turbulence Convected at High Speeds," *Philosophical Transactions of the Royal Society of London,* Ser. A, Vol. 255, 1963.

[3] Ribner, H.S., "Eddy-Mach Wave Noise from a Simplified Model of a Supersonic Mixing Layer," SP-207, 1969, NASA, pp. 53-61.

[4] Liu, J.T.C., "Developing Large-Scale Wavelike Eddies and the Near Jet Noise Field," *Journal of Fluid Mechanics,* Vol. 62, Pt. 3, 1974, pp. 437-464.

[5] Tam, C.K.W., "On the Noise of a Nearly Ideally Expanded Supersonic Jet," *Journal of Fluid Mechanics,* Vol. 51, Pt. 1, 1972, pp. 69-95.

[6] Salant, R.F., Zaic, G.F., and Kolesar, R.R., "Holographic Study of the Mach Wave Field Generated by a Supersonic Turbulent Jet," *Proceedings of the Purdue Noise Control Conference,* 1971, Lafayette, Ind.

[7]Ozkul, A., "Investigation of Acoustic Radiation from Supersonic Turbulent Jets by Double-Pulse Holographic Interferometry," Ph.D. thesis, 1974, George Washington Univ., Washington, D.C.

[8]Potter, R.C., "An Investigation to Locate the Acoustic Sources in a High Speed Jet Exhaust Stream," TR WR 68-4, 1968, Wyle Laboratories, Washington, D.C.

[9]McGregor, G.R. and Simcox, C.D., "The Location of Acoustic Sources in Jet Flows by Means of the Wall Isolation Techniques," *AIAA* Paper 73-1041, 1973.

[10]Grosche, F.R., "Untersuchunger zur Lärmentwicklung Turbulenter Freistrahlen, Teil IV, Zur Verteilung der Schallquellen in Turbulenten Strahlen" *AVA-Bericht 68 A 20,* 1968.

[11]Laufer, J., Kaplan, R.E., and Chu, W.T., "Acoustic Modeling of the Jet Noise Abatement Problem," *Proceedings of the Interagency Symposium in Transportation Noise,* 1973, Standard Univ., Stanford, Calif.

[12]Ffowcs Williams, J.E., "Impulsive Sources of Aerodynamic Sound," *AGARD Conference Proceedings on Noise Mechanisms,* No. 131, 1973, pp. 1A-1-to 1A-23.

[13]Schlinker, R.H., "Supersonic Jet Noise," USCAE 127, 1975, Univ. of Southern Califronia.

[14]Chu, W.T. and Kaplan, R.E., "A Diagnostic Tool for Jet Noise Strength Distribution Measurement," USCAE 128, 1975, Univ. of Southern California.

[15]Kao, K., "Subsonic Jet Noise Measurements by Means of a Directional Microphone System," Ph.D. Thesis, 1973, Univ. of Southern California, Los Angeles, Calif.

[16]Chu, W.T., Laufer, J., and Kao, K., "Noise Source Distribution in Subsonic Jets," *Proceedings of the 1972 International Conference on Noise Control Engineering,* 1072, Washington, D.C., pp. 472-476.

[17]Schlinker, R.H., Petersen, R.A., and Kaplan, R.E., "Enchancement of Directional Microphone Measurements," AIAA Paper 73-1040, 1973.

[18]Lighthill, M.J., "On Sound Generated Aerodynamically, I. General Theory," *Proceedings of the Royal Society* A211, 1952, pp. 564-587.

[19]Crow, S.C., "Acoustic Gain of a Turbulent Jet," *Bulletin of the American Physical Society,* Vol. IE6, 1972.

[20]Lush, P.A. and Burrin, R.H., "An Experimental Investigation of Jet Noise Variation with Velocity and Temperature," AFAPL-TR-72-53, Vol. V, 1972, Lockheed.

[21]Nagamatsu, H.T., Sheer, R.E., Jr., and Gill, M.S., "Flow and Acoustic Characteristics of Subsonic and Supersonic Jets from Convergent Nozzle," AIAA Paper 70-802, 1970.

[22]Chu, W.T., Kaplan, R.E., and Laufer, J., "Axial Source Strength Distribution in Subsonic Jets," USCAE 129, 1975, Univ. of Southern California.